Multilevel Diode-Clamped Converter for Photovoltaic Generators With Independent Voltage Control of Each Solar Array

Sergio Busquets-Monge, *Member, IEEE*, Joan Rocabert, Pedro Rodríguez, *Member, IEEE*, Salvador Alepuz, *Member, IEEE*, and Josep Bordonau, *Member, IEEE*

***Abstract*—In photovoltaic (PV) power systems where a set of series-connected PV arrays (PVAs) is connected to a conventional two-level inverter, the occurrence of partial shades and/or the mismatching of PVAs leads to a reduction of the power generated from its potential maximum. To overcome these problems, the connection of the PVAs to a multilevel diode-clamped converter is considered in this paper. A control and pulsewidth-modulation scheme is proposed, capable of independently controlling the operating voltage of each PVA. Compared to a conventional two-level inverter system, the proposed system configuration allows one to extract maximum power, to reduce the devices voltage rating (with the subsequent benefits in device-performance characteristics), to reduce the output-voltage distortion, and to increase the system efficiency. Simulation and experimental tests have been conducted with three PVAs connected to a four-level three-phase diode-clamped converter to verify the good performance of the proposed system configuration and control strategy.**

***Index Terms*—Four-level three-phase diode-clamped dc–ac converter, multilevel, photovoltaic-array (PVA) voltage control, photovoltaic (PV) energy, pulsewidth modulation, renewable energy, virtual vectors.**

I. Introduction

In RECENT years, there has been an increasing interest in electrical power generation from renewable-energy sources, such as photovoltaic (PV) or wind-power systems [1], [2]. The benefits of power generation from these sources are widely accepted. They are essentially inexhaustible and environmentally friendly.

Among the different renewable-energy sources possible to obtain electricity, solar energy has been one of the most active research areas in the past decades, both for grid-connected and stand-alone applications [3]–[9]. The installed PV power has been increasing in the past, and a more significant increase is expected in the near future, owing to the potential advances in the PV conversion technology and the reduction in cost-per-watt that a large-scale production will bring about [10]. The exponential rate of growth in the worldwide cumulative PV capacity since 1992 is mainly due to grid-connected applications. According to one of the latest reports from the International Energy Agency on Photovoltaic Power Systems (IEA PVPS T1-16:2007), 90% of the 5.7 GW of PV cumulative capacity in the IEA PVPS member countries belongs to grid-connected systems [11].

The solar panel is the basic module converting the irradiated solar energy into electricity. The power generated by the solar panel depends on the solar power incident on the panel, the panel temperature, and the operating panel voltage. The power capacity of standard solar panels is usually a few hundred watts peak (Wp), at operating dc voltages ranging from 15 to 35 V.

In grid-connected systems, the panels needed to reach the required power levels are usually arranged in strings (series connection), where all modules in the string drive the same current. PV systems at rated powers above tens of kilowatts employing centralized three-phase power inverters usually assemble several strings in parallel. In such systems, the high efficiency of the power-processing stage contrasts with the nonoptimal operation tracking the maximum power point (MPP) of the PV plant. PV systems at lower power levels usually consist of a single- or three-phase inverter processing power from a single PV string. Three-phase inverters deliver constant power to the grid, which allows one to use smaller dc capacitors than in the single-phase case. Reducing the dc capacitance allows one to reduce the cost and to improve the reliability and lifetime of the whole system.

Even though single-string PV inverters enable a better MPP tracking (MPPT) than centralized inverters, an optimal operation is not achieved. PV strings usually comprise of 20–30 modules having a total length of 15–25 m. Shading, dust, and disparity in panel aging (yellowing) cause differences in the I–V characteristics of the modules of the string, which gives rise to several local MPPs in the string P–V characteristic. Fig. 1(a) shows the I–V characteristics of two Isofoton I-165 panels under different irradiance levels: 1000 and 250 W/m^2 (dashed lines). The solid line represents the I–V characteristic of the small PV string resulting from the series connection of both panels. The modeling procedure in [12] has been followed to obtain this figure. Fig. 1(b) shows the P–V characteristic of each individual panel and the string. It can be observed that the string MPP operating under the aforementioned nonuniform

Manuscript received October 16, 2007; revised March 7, 2008. This work was supported by the Ministerio de Educación y Ciencia, Spain, under Grant TEC2005-08042.

S. Busquets-Monge, J. Rocabert, S. Alepuz, and J. Bordonau are with the Department of Electronic Engineering, Technical University of Catalonia, 08028 Barcelona, Spain (e-mail: sergio.busquets@upc.edu).

P. Rodríguez is with the Department of Electrical Engineering, Technical University of Catalonia, 08222 Terrassa, Spain (e-mail: prodriguez@ee.upc.edu).

Color versions of one or more of the figures in this paper are available online at http://ieeexplore.ieee.org.

Digital Object Identifier 10.1109/TIE.2008.924011

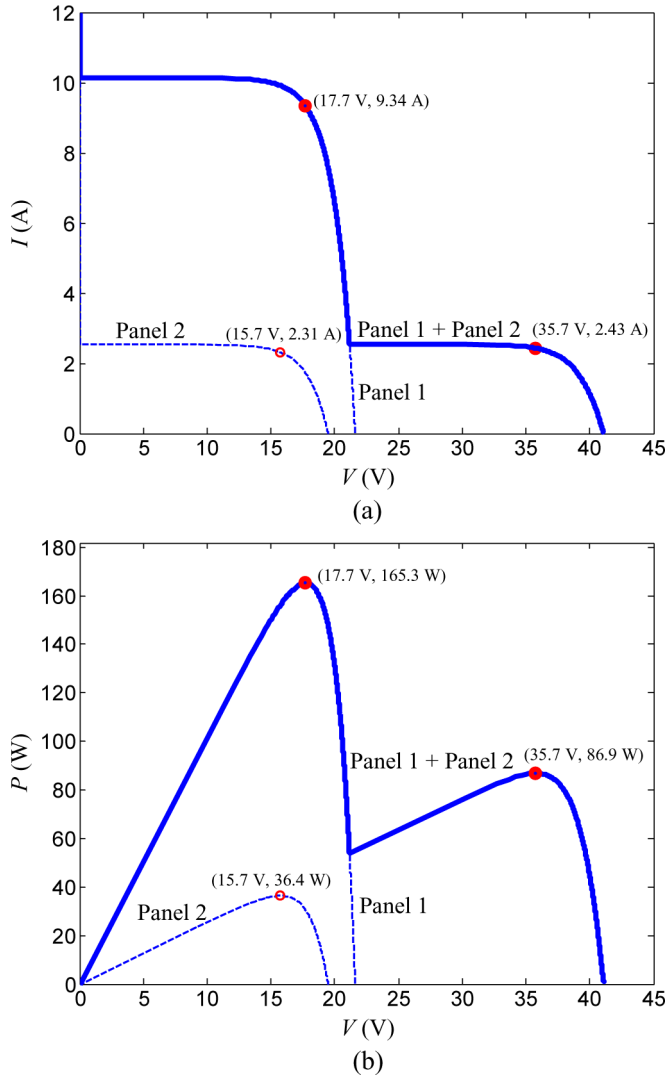

Fig. 1. Characteristics of a small string consisting of two Isofoton I-165 PV modules under different solar irradiance levels ($G_1 = 1000$ W/m^2 and $G_2 = 250$ W/m^2) and an ambient temperature $T_{\rm amb} = 25$ °C. (a) Current versus voltage. (b) Output power versus voltage.

irradiation conditions occurs at a string voltage of 17.7 V and a string current of 9.34 A. Panel 2, receiving a low irradiance level, is not able to drive the string current at the MPP and its bypass diode conducts, avoiding hot-spot effects.

PV inverters use MPPT algorithms to maximize the energy yield. Hill-climbing, perturb and observe, incremental conductance, fractional open-circuit voltage and short-circuit current, fuzzy theory, and genetic algorithms are some of the MPPT techniques discussed and compared in [13]. Some of these techniques are rather complex, and they sometimes converge to a local maximum, which is not the true string MPP. This can occur if, for example, in the two-panel string previously presented, both panels are initially operating at the same irradiance level, and then, the irradiance level on one of them changes noticeably. In the example of Fig. 1(b), an unrefined MPPT technique would bring the system to the local maximum (86.9 W) instead of the global maximum (165.3 W).

Several MPPT techniques designed to operate properly under partially shaded insolation conditions have been reported in the literature [14], [15]. Even though these techniques achieve maximum energy yield of a two-pole PV string, this does not mean that an optimal use of the different string PV modules is achieved. In the partially shaded two-panel string described in Fig. 1, at the MPP (17.7 V, 165.3 W), panel 2 is short-circuited by its by-pass diode. Panel 2 no longer acts as a generator. In fact, considering the voltage drop across the by-pass diode, it behaves as a load. Additionally, the reduction in the string voltage needed to reach the MPP may not be acceptable according to the system specifications. If an independent control of both string panels were possible, allowing different currents and voltages at each panel, the power generated by panel 2 could reach 36.4 W, which would represent an increase of 22% in the energy yield. The increase in energy yield would rise to 40% if the irradiance level of panel 2 were 500 W/m^2. On the other hand, the string voltage at the MPP would increase (33.4 V, Fig. 1).

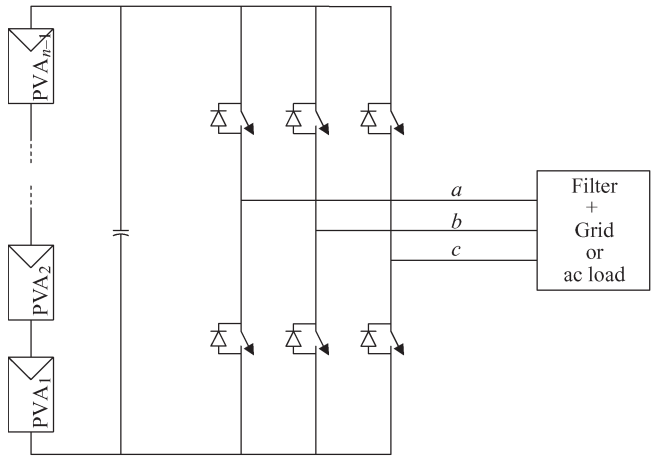

Fig. 2. Connection of $n-1$ series-connected PVAs to the grid (or ac load) through a conventional two-level three-phase inverter.

In some countries, there are national standards imposing the galvanic isolation of the PV generator under certain operating conditions, e.g., if a maximum dc-link voltage limit is exceeded. In other countries, double grounding is required, which almost always calls for galvanic isolation. This galvanic isolation can be introduced at the dc side, with a high-frequency transformer as part of a dc–dc converter, or at the output ac side, with a bulky low-frequency transformer. These additional components increase the cost and size of the whole system and decrease the overall efficiency. A higher efficiency, smaller size and weight, and a lower price for the system are possible when the isolation transformer can be omitted.

Fig. 2 shows a conventional transformerless two-level three-phase inverter used to convert the panels dc power into ac. The panels are grouped into $n-1$ series-connected PV arrays (PVAs), each one formed by one or more panels interconnected anyhow (series and/or parallel). Note that galvanic isolation would be required in some countries if the dc-link voltage exceeds a given maximum, as discussed earlier. Since the same current must flow through all PVAs, the system does not allow the independent control of the operating voltage of each individual PVA. As a result, the power extracted cannot be maximized.

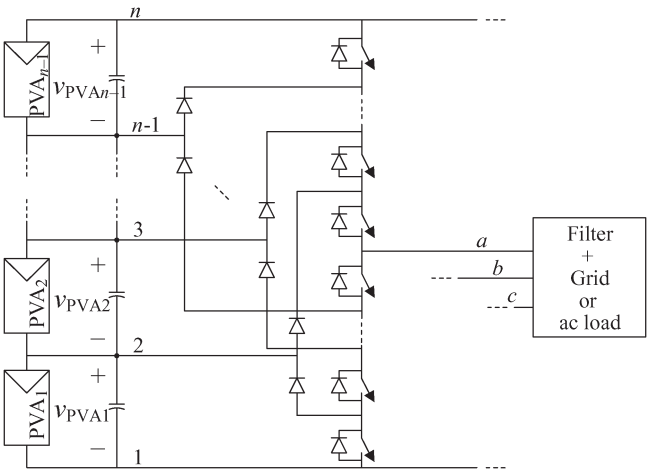

Fig. 3. Connection of $n-1$ series-connected PVAs to the grid (or ac load) through a n-level three-phase diode-clamped inverter.

To solve this problem, some authors propose the inclusion of additional circuitry to the system in Fig. 2 [3], [16], allowing the flow of different current values through each PVA, and hence, enabling the independent control of each PVA voltage to operate them at their MPP.

Other authors propose the replacement of the conventional two-level converter by a multilevel converter [17]–[22].

Besides being able to maximize the power obtained from the PVAs, the multilevel converter usually presents the advantages of reducing the device voltage stress, being more efficient, and generating a lower output ac-voltage harmonic distortion. Among the following three main families of multilevel converters: diode-clamped, capacitor-clamped, and cascaded H-bridge [23], [24], the latter is usually considered in the literature for PV applications [18]–[21].

In this paper, diode-clamped topologies are considered due to their simplicity. They present a lower count of active power devices per PVA than cascaded H-bridge topologies. The general case of an n-level diode-clamped converter is shown in Fig. 3. The control for this type of multilevel converters to guarantee optimum PVA voltage and a low distorted output current is not obvious. This paper presents a proposal for such control, and its performance is analyzed through simulation and experiments.

This paper is organized as follows. Section II presents the control and modulation scheme proposed for independent voltage control. Sections III and IV analyze the performance of this scheme, in the particular case of a four-level three-phase diode-clamped inverter, through simulation and through experiments conducted in a PV facility. Finally, Section V outlines the conclusion.

II. Control and Modulation Scheme for Independent PVA Voltage Control

The n-level three-phase system in Fig. 3 is considered here. For the sake of simplicity, a three-phase passive load is assumed. The essence of the control and modulation does not change if the system is connected to the grid. Each converter phase (a, b, and c) can be connected to any of the n available dc-link points $(1, 2, \ldots, \text{and } n)$. Let us designate as d_{xy} the duty ratio of the phase x connection to the dc-link point y, within a switching cycle of period $T_s(= 1/f_s)$.

Reference [25] presents a control and modulation scheme capable of guaranteeing equal dc-link capacitor voltages for n-level diode-clamped converters fed by a single dc voltage supply. This scheme is adapted here to PV applications, where unequal PVA command voltages are possible. Hence, the scheme proposed here can be regarded as a generalization of the original one. Fig. 4 shows a diagram describing its structure. The three main blocks are commented in the following sections.

A. Total DC-Link Voltage Control

Variables $v_{\text{PVA}1}, v_{\text{PVA}2}, \ldots, v_{\text{PVA}n-1}$ are the sensed PVA voltages (dc-link capacitor voltages). Let us designate $v^*_{\text{PVA}1}, v^*_{\text{PVA}2}, \ldots, v^*_{\text{PVA}n-1}$ as the corresponding command voltages. These command voltages can be determined by a given MPPT algorithm, such as the algorithm presented in [16]. This MPPT strategy only requires the measurement of the power transferred to the grid (or load) through the sensing of two phase currents (if the addition of the three phase currents is equal to zero) and two line-to-line voltages (see Fig. 5). There is no need to sense the PVA currents. The optimum value of the PVA command voltages is then obtained through a hill-climbing algorithm as detailed in [16].

The total dc-link voltage value can be computed from the sensed PVA voltages as

$$v_{n1} = \sum_{k=1}^{n-1} v_{\text{PVA}k}. \tag{1}$$

The sensed dc-link voltage value is compared to the corresponding command value. The resulting error is processed through a compensator and a limiter to obtain the value of modulation index m. Variables $m(\in [0, 1])$ and θ are the normalized length and angle, respectively, of a rotating vector (reference vector) representing the desired three-phase output voltage.

In the case of a grid connection, the output of this control loop would represent the direct component of the phase currents instead of m. Then, two additional current loops would be introduced to determine the desired direct and quadrature components of the reference vector.

B. Unbalance Control

For each internal dc-link point $j(= 2, 3, \ldots, n-1)$, two partial dc-link voltages are defined

$$v_{j1} = \sum_{k=1}^{j-1} v_{\text{PVA}k}$$

$$v_{nj} = \sum_{k=j}^{n-1} v_{\text{PVA}k}. \tag{2}$$

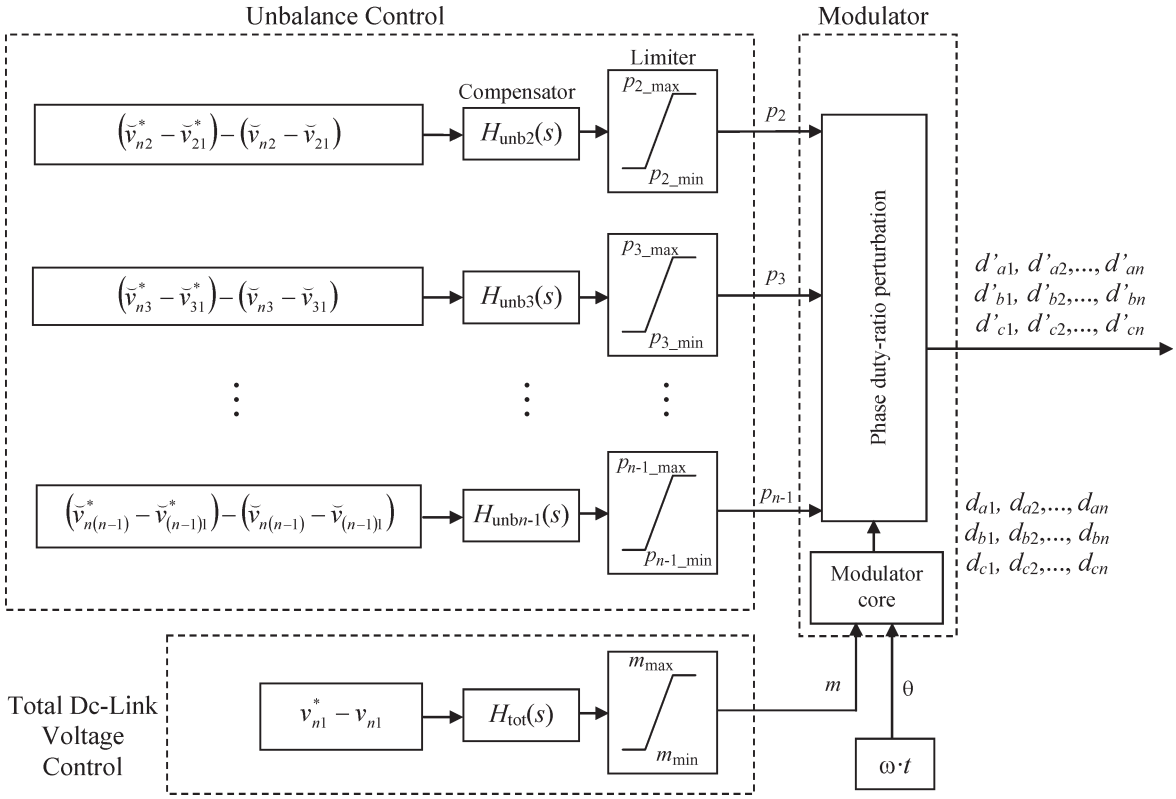

Fig. 4. Control and modulator structure.

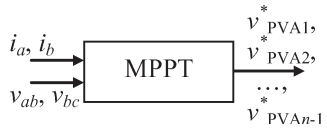

Fig. 5. MPPT algorithm inputs and outputs.

These values can be normalized by dividing by the corresponding number of added PVA voltages

$$\breve{v}_{j1}=\frac{\sum_{k=1}^{j-1} v_{\text{PVA}k}}{j-1}$$
$$\breve{v}_{nj}=\frac{\sum_{k=j}^{n-1} v_{\text{PVA}k}}{n-j}. \quad (3)$$

For each internal dc-link point j, we compute the difference between the corresponding normalized sensed partial voltages, and we compute the same difference for the command values. The error is then processed through a compensator and a limiter to obtain variables p_j, which indicate the required control effort, extracting/injecting current from/into dc-link point j, to achieve the desired partial voltage unbalance.

The combination of the unbalance control block and the total dc-link voltage control block guarantees that the actual PVA voltages will have a value in steady state equal to the corresponding command. The control of these voltages is critical in order to operate the PV power system at the MPP. A given MPPT algorithm will be in charge of finding the optimum set of values. However, this control capability can also be useful for other purposes, such as in islanding detection. Reference [26] presents a review of the islanding detection methods for PV utility-interactive power systems. All methods resident in the inverter (passive and active) can be applied to the inverter system shown in Fig. 3. In particular, with the proposed modulation and control, those methods requiring a variation of the power delivered by the PV power system can be implemented in a controlled manner by simply modifying the PVA voltage commands. An interesting scheme consists of increasing the voltage command of some PVAs and decreasing the voltage command of other PVAs in the same amount so that the total dc-link voltage does not change. This scheme can be used to inject a specific current harmonic in the "detection of impedance at a specific frequency" method or to decrease the active power delivered in the "Sandia voltage shift" method until the undervoltage protection is activated.

C. Modulator

The modulator contains the following two blocks: the modulator core and the phase duty-ratio perturbation block.

The modulator core generates the phase duty-ratio variables from the information of the reference vector length (m) and angle (θ). This block can contain any virtual-vector-based modulation strategy, such as the strategies presented in [27] and [28]. These modulation schemes will not produce low-frequency distortions in the output three-phase voltages, even operating under unequal PVA voltages, as will be seen in the next section. This is a critical property in order to be able to operate under unequal PVA voltages.

The phase duty-ratio perturbation block is in charge of modifying (perturbing) the phase duty ratios in order to recover

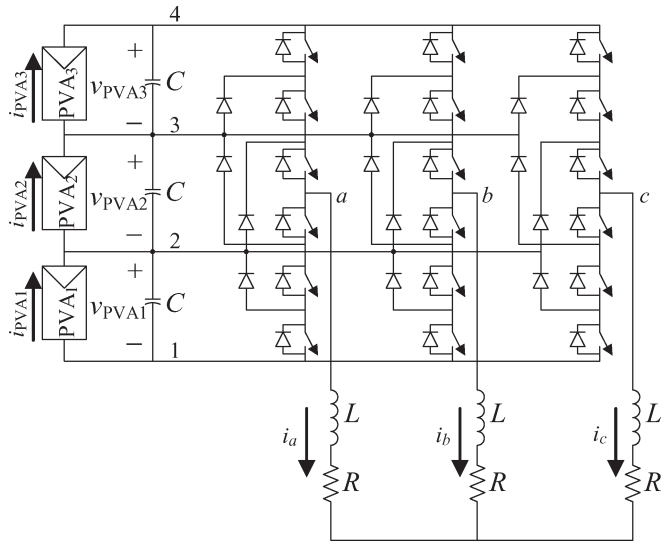

Fig. 6. Connection of three series-connected PVAs to a passive R–L load through a four-level three-phase diode-clamped inverter.

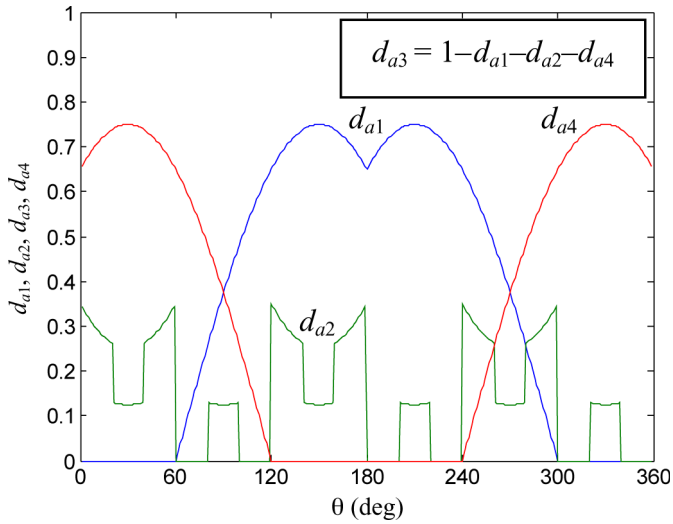

Fig. 7. Phase a duty-ratio pattern ($m = 0.75$).

the commanded PVA voltage differences in case the sensed voltages do not present the same differences. Any of the perturbation schemes reported in [25] performs satisfactorily.

The resulting modified phase duty ratios $(d'_{a1}, \ldots, d'_{cn})$ are finally sent to a distributor block to symmetrically distribute the connections of each phase to each of the dc-link points within a switching cycle and generate the switch control signals [27], [28].

III. Simulation Results

Simulations have been carried out in MATLAB–Simulink to study the performance of the proposed control and modulation scheme. The particular system shown in Fig. 6 is modeled. Three PVAs are connected to a passive load through a four-level three-phase diode-clamped inverter. Each PVA contains four series-connected 12-V 165-Wp PV panels (Isofoton I-165). The panel model in [29] has been tuned to the specific modules considered here.

The virtual-vector-based pulsewidth modulation for the four-level converter presented in [28] is employed as the modulator core. The Appendix contains the algorithm used to implement this modulation scheme. Fig. 7 shows the corresponding phase a duty-ratio pattern for $m = 0.75$. Perturbation scheme C in [25] is used as the phase duty-ratio perturbation scheme, since this is the best solution for three-phase systems. The Appendix also contains the algorithm used to implement this perturbation scheme.

The controller transfer functions and parameters for all simulations are

$$H_{\mathrm{unb2}}(s) = H_{\mathrm{unb3}}(s) = 10 \cdot \frac{(s + 2\pi \cdot 0.01)}{s \cdot (s + 2\pi \cdot 100)}$$

$$H_{\mathrm{tot}}(s) = -100 \cdot \frac{(s + 2\pi \cdot 5)}{s \cdot (s + 2\pi \cdot 500)}$$

$$[p_{2\_\min}, p_{2\_\max}] = [p_{3\_\min}, p_{3\_\max}] = [-0.1, 0.1]$$

$$[m_{\min}, m_{\max}] = [0, 1]. \quad (4)$$

Fig. 8 shows the simulation results in steady state for the output voltages and currents under the following two conditions: equal [Fig. 8(a)] and unequal PVA voltages [Fig. 8(b)]. Fig. 8(b) shows that, even under unequal PVA voltages, the output voltage (and hence, the output current) does not present any distortion at frequencies below the first group of harmonics around the switching frequency. This is a particular property of the virtual-vector modulator core used. It does not produce low-frequency distortions in the output line-to-line voltages and phase currents regardless of the value of the capacitor voltages. This occurs because, in every switching cycle, all PVA voltages are used to synthesize the output voltage. Hence, the differences cancel out in every switching cycle and do not affect the frequency spectrum of the voltages below the switching frequency. There are small differences in the high-frequency spectrum, but the total harmonic distortion (THD) is similar in both cases.

Figs. 9 and 10 show the transient PVA voltages and phase currents under a step in the command PVA voltages. The control is able to drive the voltages effectively to the new set of command values. There is no noticeable distortion in the output phase currents during the transient. Note that the peak of the phase currents does not change despite changing the power delivered by each individual PVA, because in the particular conditions simulated here, the total amount of power delivered by all three PVAs remains the same.

The control scheme presented in Section II aims to regulate independently the PVA voltages for all possible set of irradiation values $\mathbf{G} = (G_{\mathrm{PVA1}}, G_{\mathrm{PVA2}}, \ldots, G_{\mathrm{PVA}n-1})$, where $G_{\mathrm{PVA}i}$ is the solar irradiation over PVA_i. If all the irradiation values are similar, the control effort required (absolute value of variables p_i, in steady state) is very small, and the regulation can be achieved, in general, for any value of the modulation index $m \in (0, 1)$. However, as the differences in the irradiation values increase, the control effort required to obtain the desired regulation increases. This control effort is limited by the limits in the phase duty-ratio values. Moreover, this control effort limit is more restrictive as the modulation index increases. As a result, the range of values of vector $\mathbf{G}$ for which regulation is possible

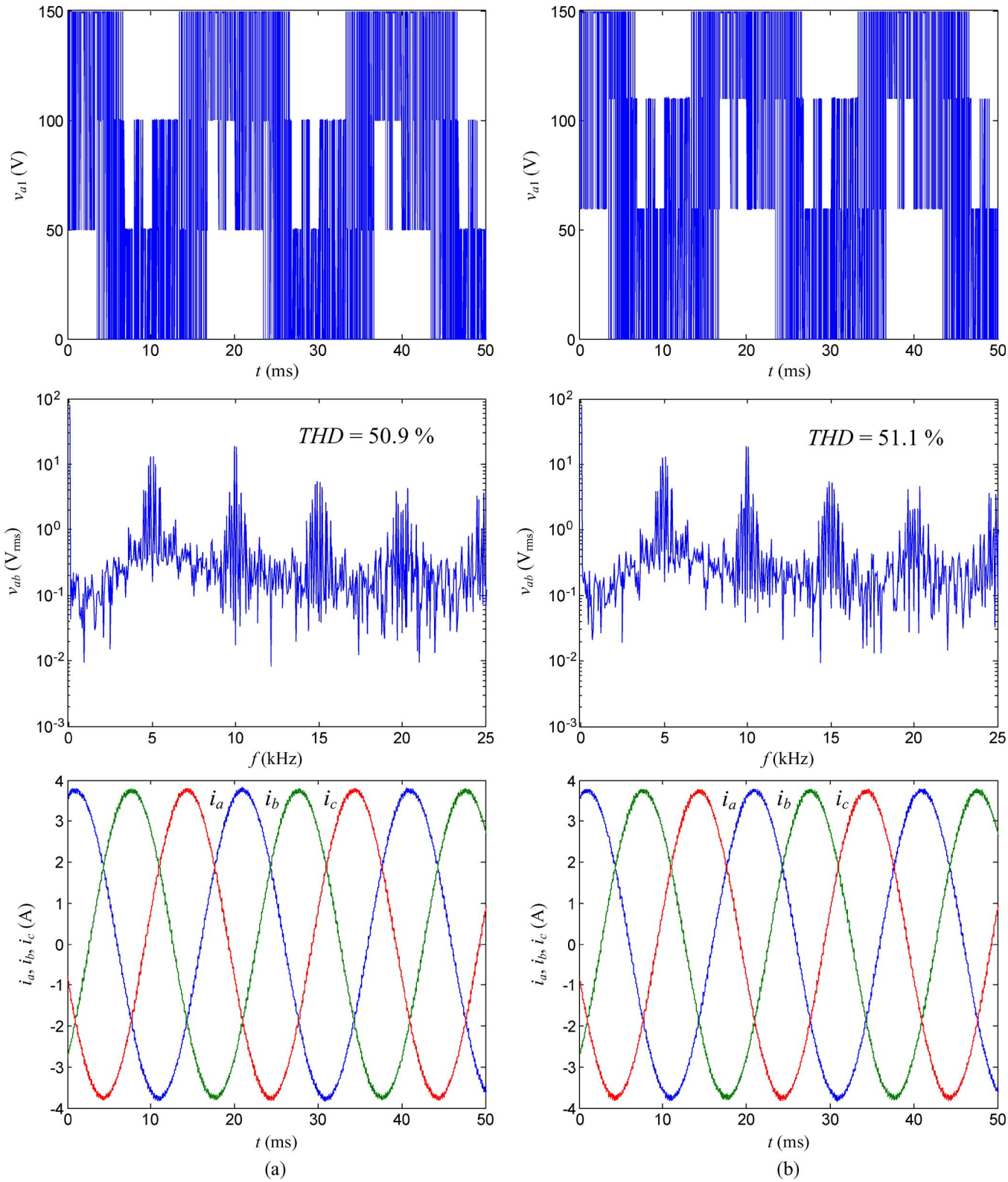

Fig. 8. Simulation results for phase voltage v_{a1}, fast Fourier transform of line-to-line voltage v_{ab}, and phase currents under the following conditions: $(G_{\mathrm{PVA1}}, G_{\mathrm{PVA2}}, G_{\mathrm{PVA3}}) = (230, 230, 230)$ W/m^2, $T_{\mathrm{amb}} = 25$ °C, $C = 570$ μF, $R = 16.5$ Ω, $L = 15$ mH, and $f_{\mathrm{s}} = 5$ kHz. (a) $(v^*_{\mathrm{PVA1}}, v^*_{\mathrm{PVA2}}, v^*_{\mathrm{PVA3}}) = (50, 50, 50)$ V. (b) $(v^*_{\mathrm{PVA1}}, v^*_{\mathrm{PVA2}}, v^*_{\mathrm{PVA3}}) = (60, 50, 40)$ V.

decreases as the modulation index increases. For instance, in the system configuration shown in Fig. 6, with $G_{\mathrm{PVA2}} = G_{\mathrm{PVA3}} = 500$ W/m^2, $T_{\mathrm{amb}} = 25$ °C, $C = 570$ μF, $L = 1$ mH, $f_s = 5$ kHz, and R is adjusted to achieve $m \cong 0.5$, regulation is possible for $G_{\mathrm{PVA1}} \in [10, 1000]$ W/m^2. However, if $m \cong 0.9$ regulation is only possible for $G_{\mathrm{PVA1}} \in [400, 550]$ W/m^2. These limitations might be partially overcome with a better suited phase duty-ratio perturbation scheme [25]. In any

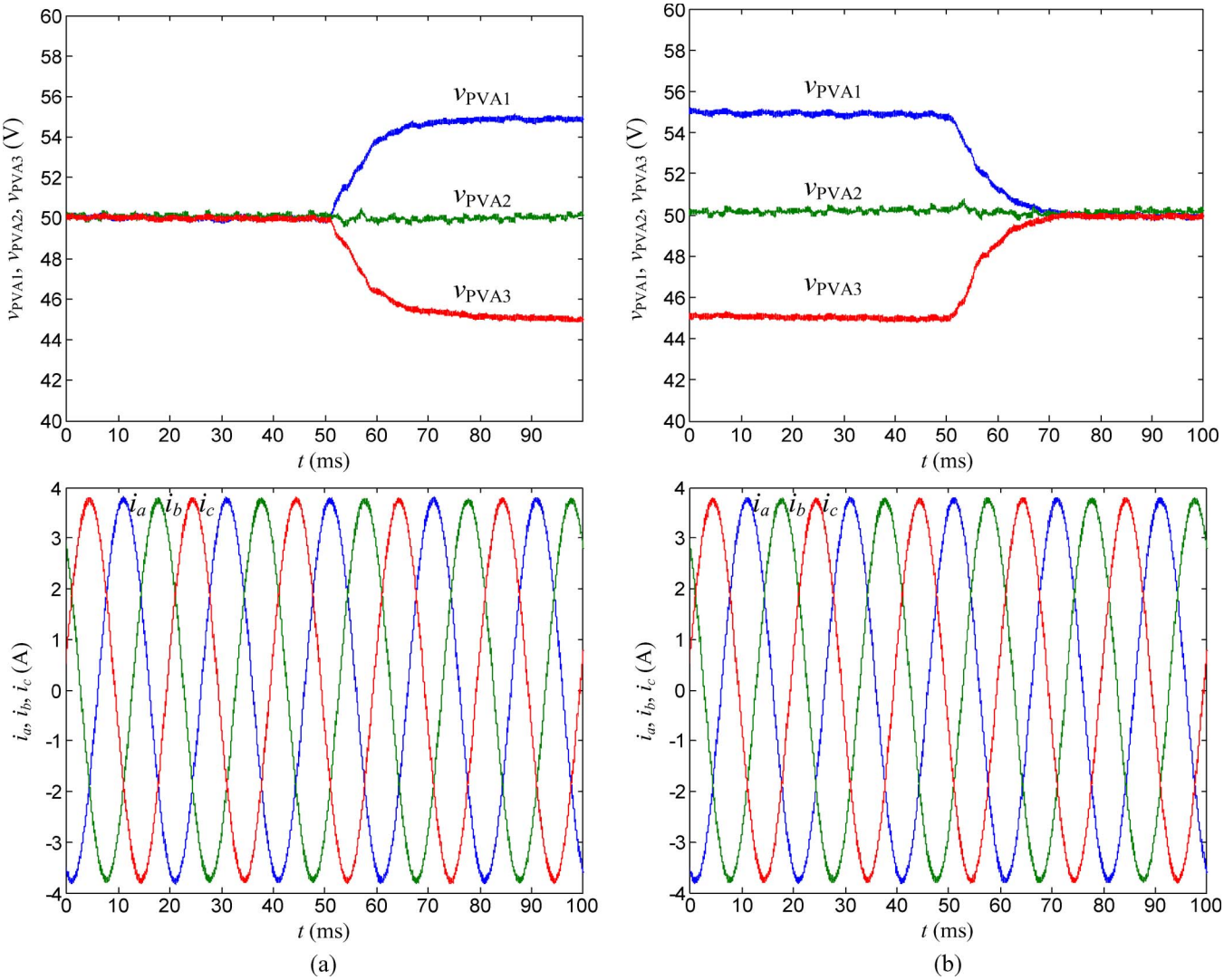

Fig. 9. Simulated transients under a step in the PVAs voltage commands at $t = 50$ ms. Same conditions as in Fig. 8. (a) Step from $(v^*_{\mathrm{PVA1}}, v^*_{\mathrm{PVA2}}, v^*_{\mathrm{PVA3}}) = (50, 50, 50)$ V to $(v^*_{\mathrm{PVA1}}, v^*_{\mathrm{PVA2}}, v^*_{\mathrm{PVA3}}) = (55, 50, 45)$ V. (b) Step from $(v^*_{\mathrm{PVA1}}, v^*_{\mathrm{PVA2}}, v^*_{\mathrm{PVA3}}) = (55, 50, 45)$ V to $(v^*_{\mathrm{PVA1}}, v^*_{\mathrm{PVA2}}, v^*_{\mathrm{PVA3}}) = (50, 50, 50)$ V.

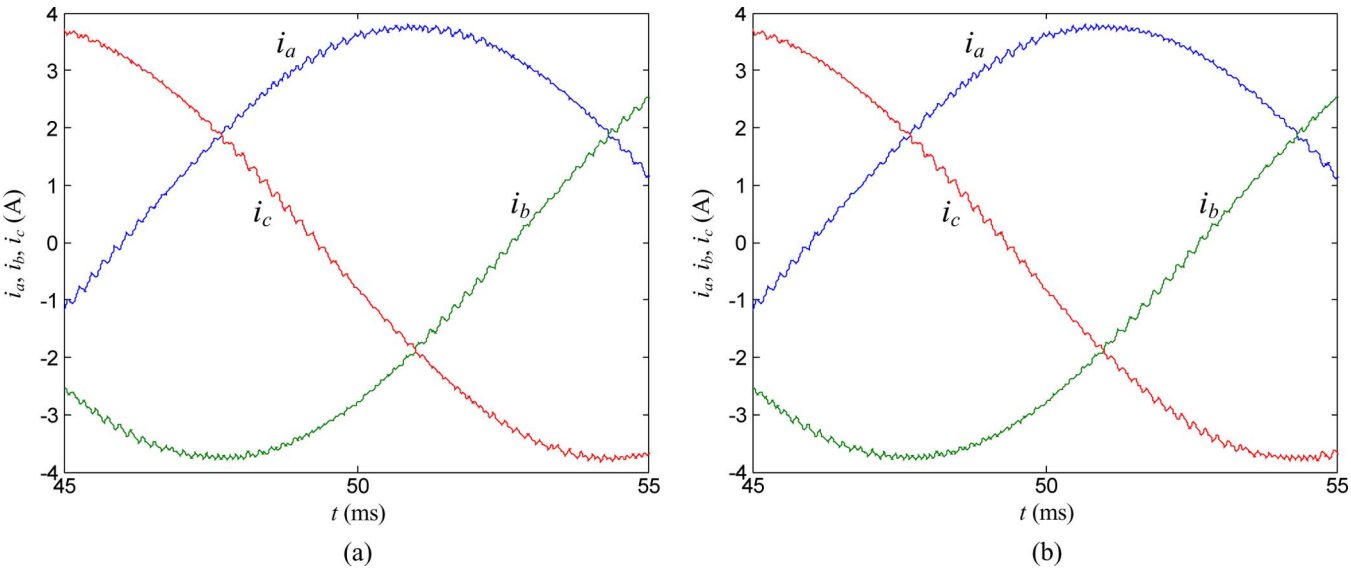

Fig. 10. Zoom of Fig. 9.

Fig. 11. PVAs PVA_1, PVA_2, and PVA_3 employed in the experiments.

case, and to benefit from wider control capabilities, it is recommended to design the system to operate at a moderate modulation-index value.

IV. Experimental Results

Experimental tests have been conducted with the system configuration shown in Fig. 6, under the same conditions and controller settings detailed in the previous section. Fig. 11 shows the three PVAs employed, each one formed by four series-connected Isofoton I-165 PV panels. The control and modulator computations to obtain the nine independent phase duty ratios are performed by the embedded PowerPC (PPC 604e) of dSpace DS1103. This information is sent to an Altera EPF10K70 programmable logic device in charge of generating the eighteen switch control signals. The average time required for the analog-to-digital conversion and PowerPC processing is 40 μs. In the Altera device, 1365 logic cells are used. In a commercial product, a single digital-signal processor could be selected to perform all these functions.

Fig. 12 shows the converter output phase voltage v_{a1} and phase currents in steady state under equal [Fig. 12(a)] and unequal [Fig. 12(b)] PVA voltages. No noticeable low-frequency distortion appears in the line currents in both cases, confirming the simulation results shown in Fig. 8.

Fig. 13 shows the experimental results in the same conditions shown in Fig. 9. It can be seen that there is a fairly good agreement between simulations and experiments. The phase current level is slightly lower in the experiments than predicted, because a lossless model has been employed for simulation. Additionally, the model does not take into account phenomena such as dust over the modules.

Finally, Table I presents experimental results with regard to PVA voltages, PVA currents, PVA power (p_{PVA}), and total PV output power (P_{o}) under a controlled shading of PVA_1 with the unbalance control deactivated and activated. Without the unbalance control, the shaded PVA limits the current flowing through the remaining PVAs. The output power obtained $(P_{\mathrm{o}} = 426.8\ \mathrm{W})$ is the same as with a two-level converter for the same total dc-link voltage (the expected MPP with a two-level converter would produce $P_{\mathrm{o}} = (64 + 71 + 69)\ \mathrm{V} * 2.2\ \mathrm{A} = 448.8\ \mathrm{W}$). In the four-level converter, the activation of the unbalance control allows one to search for the MPP of each PVA, leading to a 30% increase in the total output power.

V. Conclusion

A control and modulation scheme for the connection of a set of PVAs to a multilevel diode-clamped three-phase inverter has been presented. The scheme allows one to independently set each PVA voltage to its MPP without diminishing the quality of the output voltages. This feature, and compared to a conventional system using a two-level inverter, allows one to increase the power extracted, particularly under partial shades covering the PV facility or in case of mismatched PVAs. Additionally, the use of multilevel diode-clamped converters reduces the voltage rating of the devices, allows one to operate without transformers to step-up the voltage, reduces the output harmonic distortion, and increases the efficiency of the power conversion.

The control presented can also be used for single- and two-leg systems, with the selection of a proper modulator.

Appendix I
Four-Level Three-Phase Modulation Algorithm

A. Modulator Core

An algorithm to compute the phase duty ratios of a virtual-vector-based pulsewidth modulation for the four-level three-phase diode-clamped dc–ac converter follows.

The first step consists of transforming the so-called reference vector, $\mathbf{V}_{\mathrm{ref}} = (V_{\mathrm{ref}\alpha}, V_{\mathrm{ref}\beta})$, into the equivalent vector located in the first sextant of the converter space-vector diagram

$$
\begin{aligned}
&V_{\mathrm{ref}\alpha} = m \cdot \cos(\theta)\\
&V_{\mathrm{ref}\beta} = m \cdot \sin(\theta)\\
&sextant = 1\\
&\mathbf{M}_{-60} = \begin{bmatrix} 1/2 & \sqrt{3}/2 \\ -\sqrt{3}/2 & 1/2 \end{bmatrix}\\
&\text{while } \Big((V_{\mathrm{ref}\beta} < 0) \text{ or } (V_{\mathrm{ref}\beta} > \sqrt{3} \cdot V_{\mathrm{ref}\alpha}) \Big) \{\\
&\quad sextant = sextant + 1\\
&\quad \begin{bmatrix} V_{\mathrm{ref}\alpha} \\ V_{\mathrm{ref}\beta} \end{bmatrix} = \mathbf{M}_{-60} \cdot \begin{bmatrix} V_{\mathrm{ref}\alpha} \\ V_{\mathrm{ref}\beta} \end{bmatrix}\\
&\}. \qquad (5)
\end{aligned}
$$

Next, the values of parameters d_1, d_2, d_3, and d_4 are computed

$$
\begin{aligned}
&d_1 = (\sqrt{3}/2) \cdot V_{\mathrm{ref}\alpha} - (1/2) \cdot V_{\mathrm{ref}\beta}\\
&d_4 = (\sqrt{3}/2) \cdot V_{\mathrm{ref}\alpha} + (1/2) \cdot V_{\mathrm{ref}\beta}\\
&\text{if} \Bigg(\left[\left(V_{\mathrm{ref}\alpha} < \frac{1}{\sqrt{3}} \right) \text{ or } \left(V_{\mathrm{ref}\beta} < \frac{2}{3} - \frac{V_{\mathrm{ref}\alpha}}{\sqrt{3}} \right) \right]\\
&\qquad \text{and } (V_{\mathrm{ref}\beta} > 1 - \sqrt{3} \cdot V_{\mathrm{ref}\alpha}) \Bigg) \{
\end{aligned}
$$

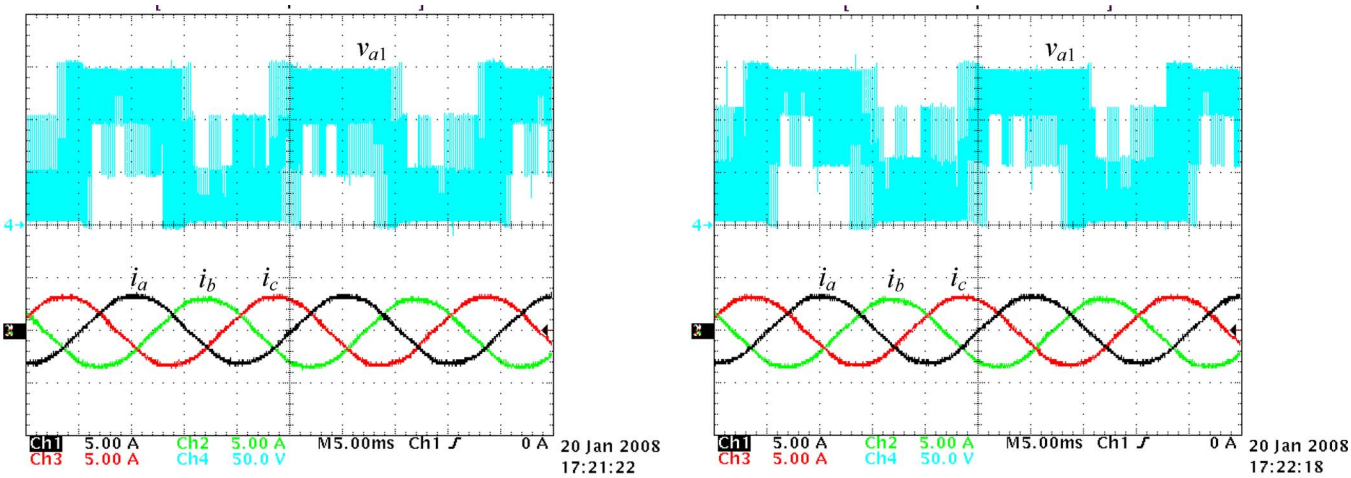

Fig. 12. Experimental results for the phase voltage v_{a1} and phase currents under the same conditions as shown in Fig. 8. (a) $(v^*_{\mathrm{PVA1}}, v^*_{\mathrm{PVA2}}, v^*_{\mathrm{PVA3}}) = (50, 50, 50)$ V. (b) $(v^*_{\mathrm{PVA1}}, v^*_{\mathrm{PVA2}}, v^*_{\mathrm{PVA3}}) = (60, 50, 40)$ V.

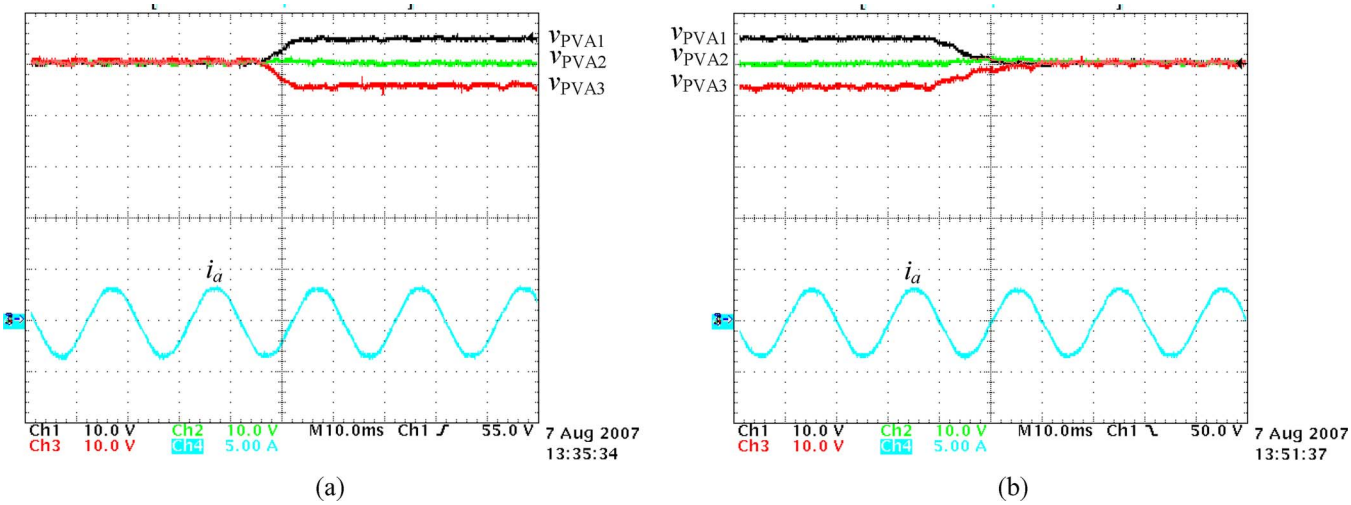

Fig. 13. Experimental transients under a step in the PVAs voltage commands. Same conditions as shown in Fig. 8. (a) Step from $(v^*_{\mathrm{PVA1}}, v^*_{\mathrm{PVA2}}, v^*_{\mathrm{PVA3}}) = (50, 50, 50)$ V to $(v^*_{\mathrm{PVA1}}, v^*_{\mathrm{PVA2}}, v^*_{\mathrm{PVA3}}) = (55, 50, 45)$ V. (b) Step from $(v^*_{\mathrm{PVA1}}, v^*_{\mathrm{PVA2}}, v^*_{\mathrm{PVA3}}) = (55, 50, 45)$ V to $(v^*_{\mathrm{PVA1}}, v^*_{\mathrm{PVA2}}, v^*_{\mathrm{PVA3}}) = (50, 50, 50)$ V.

$$
\begin{aligned}
& d_2 = 1 - d_4 \\
& d_3 = 0 \\
&\} \text{ else } \{ \\
& d_2 = (1 - d_4)/2 \\
& d_3 = (1 - d_4)/2 \\
&\}.
\end{aligned} \tag{6}
$$

Alternatively, the expressions in (7) can be used, leading to a simpler modulation scheme with greater control capabilities (all phase duty ratios of connection to an inner dc-link point are always higher than zero) at the expense of a slightly higher output THD

$$
\begin{aligned}
d_1 &= (\sqrt{3}/2) \cdot V_{\mathrm{ref}\alpha} - (1/2) \cdot V_{\mathrm{ref}\beta} \\
d_4 &= (\sqrt{3}/2) \cdot V_{\mathrm{ref}\alpha} + (1/2) \cdot V_{\mathrm{ref}\beta} \\
d_2 &= d_3 = (1 - d_4)/2.
\end{aligned} \tag{7}
$$

TABLE I
EXPERIMENTAL RESULTS WITH $(G_{\mathrm{PVA1}}, G_{\mathrm{PVA2}}, G_{\mathrm{PVA3}}) = (240, 350, 350^*)$ W/m^2

	Unbalance Control off	Unbalance Control on (at the MPP)
v_{PVA1}(V)	54	64
v_{PVA2}(V)	71	65
v_{PVA3}(V)	69	65
i_{PVA1}(A)	2.2	2.2
i_{PVA2}(A)	2.2	3.4
i_{PVA3}(A)	2.2	3.0
p_{PVA1}(W)	118.8	140.8
p_{PVA2}(W)	156.2	221.0
p_{PVA3}(W)	151.8	195.0
P_o(W)	426.8 (100%)	556.8 (130%)

*: An unintended shade was covering a small portion of PVA$_3$.

Finally, the phase duty ratios are calculated with the simple expressions in Table II.

TABLE II
PHASE DUTY-RATIO COMPUTATION

sextant	Phase duty-ratios		
	Phase *a*	Phase *b*	Phase *c*
1	$d_{a1}=0$ $d_{a2}=d_2$ $d_{a3}=d_3$ $d_{a4}=d_4$	$d_{b1}=d_1$ $d_{b2}=d_2$ $d_{b3}=d_3$ $d_{b4}=V_{\text{ref}\beta}$	$d_{c1}=d_4$ $d_{c2}=d_2$ $d_{c3}=d_3$ $d_{c4}=0$
2	$d_{a1}=V_{\text{ref}\beta}$ $d_{a2}=d_3$ $d_{a3}=d_2$ $d_{a4}=d_1$	$d_{b1}=0$ $d_{b2}=d_3$ $d_{b3}=d_2$ $d_{b4}=d_4$	$d_{c1}=d_4$ $d_{c2}=d_3$ $d_{c3}=d_2$ $d_{c4}=0$
3	$d_{a1}=d_4$ $d_{a2}=d_2$ $d_{a3}=d_3$ $d_{a4}=0$	$d_{b1}=0$ $d_{b2}=d_2$ $d_{b3}=d_3$ $d_{b4}=d_4$	$d_{c1}=d_1$ $d_{c2}=d_2$ $d_{c3}=d_3$ $d_{c4}=V_{\text{ref}\beta}$
4	$d_{a1}=d_4$ $d_{a2}=d_3$ $d_{a3}=d_2$ $d_{a4}=0$	$d_{b1}=V_{\text{ref}\beta}$ $d_{b2}=d_3$ $d_{b3}=d_2$ $d_{b4}=d_1$	$d_{c1}=0$ $d_{c2}=d_3$ $d_{c3}=d_2$ $d_{c4}=d_4$
5	$d_{a1}=d_1$ $d_{a2}=d_2$ $d_{a3}=d_3$ $d_{a4}=V_{\text{ref}\beta}$	$d_{b1}=d_4$ $d_{b2}=d_2$ $d_{b3}=d_3$ $d_{b4}=0$	$d_{c1}=0$ $d_{c2}=d_2$ $d_{c3}=d_3$ $d_{c4}=d_4$
6	$d_{a1}=0$ $d_{a2}=d_3$ $d_{a3}=d_2$ $d_{a4}=d_4$	$d_{b1}=d_4$ $d_{b2}=d_3$ $d_{b3}=d_2$ $d_{b4}=0$	$d_{c1}=V_{\text{ref}\beta}$ $d_{c2}=d_3$ $d_{c3}=d_2$ $d_{c4}=d_1$

B. Phase Duty-Ratio Perturbation

The algorithm describing the phase duty-ratio perturbation scheme for phase x, assuming $i_a+i_b+i_c=0$, is presented in (8) [25]

$$
\begin{aligned}
v_{a1} &= v_{\text{PVA1}}\cdot d_{a2} + (v_{\text{PVA1}}+v_{\text{PVA2}})\cdot d_{a3} \\
&\quad + (v_{\text{PVA1}}+v_{\text{PVA2}}+v_{\text{PVA3}})\cdot d_{a4} \\
v_{b1} &= v_{\text{PVA1}}\cdot d_{b2} + (v_{\text{PVA1}}+v_{\text{PVA2}})\cdot d_{b3} \\
&\quad + (v_{\text{PVA1}}+v_{\text{PVA2}}+v_{\text{PVA3}})\cdot d_{b4} \\
v_{c1} &= v_{\text{PVA1}}\cdot d_{c2} + (v_{\text{PVA1}}+v_{\text{PVA2}})\cdot d_{c3} \\
&\quad + (v_{\text{PVA1}}+v_{\text{PVA2}}+v_{\text{PVA3}})\cdot d_{c4} \\
v_{ac} &= v_{a1}-v_{c1} \\
v_{bc} &= v_{b1}-v_{c1} \\
pow &= i_a\cdot v_{ac} + i_b\cdot v_{bc}
\end{aligned}
$$

$$
\begin{aligned}
&\textbf{if}(p_j\cdot pow\geq 0)\{ \\
&\quad \textbf{if}\,(d_{xn}>|p_j|/(n-j))\,\{ \\
&\qquad d'_{xn}=d_{xn}-|p_j|/(n-j) \\
&\qquad d'_{x1}=d_{x1} \\
&\quad \}\textbf{else}\{ \\
&\qquad d'_{xn}=0 \\
&\qquad d'_{x1}=d_{x1}+[|p_j|/(n-j)-d_{xn}]\cdot[(n-j)/(j-1)] \\
&\quad \} \\
&\}\textbf{else}\{ \\
&\quad \textbf{if}\,(d_{x1}>|p_j|/(j-1))\,\{ \\
&\qquad d'_{x1}=d_{x1}-|p_j|/(j-1) \\
&\qquad d'_{xn}=d_{xn} \\
&\quad \}\textbf{else}\{ \\
&\qquad d'_{x1}=0 \\
&\qquad d'_{xn}=d_{xn}+[|p_j|/(j-1)-d_{x1}]\cdot[(j-1)/(n-j)] \\
&\quad \} \\
&\} \\
&d'_{xj}=(d_{x1}+d_{xj}+d_{xn})-d'_{x1}-d'_{xn}.
\end{aligned}
\tag{8}
$$

REFERENCES

[1] J. M. Carrasco, L. G. Franquelo, J. T. Bialasiewicz, E. Galvan, R. C. Portillo Guisado, M. A. M. Prats, J. I. Leon, and N. Moreno-Alfonso, "Power-electronic systems for the grid integration of renewable energy sources: A survey," *IEEE Trans. Ind. Electron.*, vol. 53, no. 4, pp. 1002–1016, Jun. 2006.

[2] F. Blaabjerg, Z. Chen, and S. B. Kjaer, "Power electronics as efficient interface in dispersed power generation systems," *IEEE Trans. Power Electron.*, vol. 19, no. 5, pp. 1184–1194, Sep. 2004.

[3] E. Roman, R. Alonso, P. Ibanez, S. Elorduizapatarietxe, and D. Goitia, "Intelligent PV module for grid-connected PV systems," *IEEE Trans. Ind. Electron.*, vol. 53, no. 4, pp. 1066–1073, Jun. 2006.

[4] W. Xiao, W. G. Dunford, P. R. Palmer, and A. Capel, "Regulation of photovoltaic voltage," *IEEE Trans. Ind. Electron.*, vol. 54, no. 3, pp. 1365–1374, Jun. 2007.

[5] W. Xiao, N. Ozog, and W. G. Dunford, "Topology study of photovoltaic interface for maximum power point tracking," *IEEE Trans. Ind. Electron.*, vol. 54, no. 3, pp. 1696–1704, Jun. 2007.

[6] W. Xiao, M. G. J. Lind, W. G. Dunford, and A. Capel, "Real-time identification of optimal operating points in photovoltaic power systems," *IEEE Trans. Ind. Electron.*, vol. 53, no. 4, pp. 1017–1026, Jun. 2006.

[7] N. Mutoh, M. Ohno, and T. Inoue, "A method for MPPT control while searching for parameters corresponding to weather conditions for PV generation systems," *IEEE Trans. Ind. Electron.*, vol. 53, no. 4, pp. 1055–1065, Jun. 2006.

[8] J.-H. Park, J.-Y. Ahn, B.-H. Cho, and G.-J. Yu, "Dual-module-based maximum power point tracking control of photovoltaic systems," *IEEE Trans. Ind. Electron.*, vol. 53, no. 4, pp. 1036–1047, Jun. 2006.

[9] R.-J. Wai, W.-H. Wang, and C.-Y. Lin, "High-performance stand-alone photovoltaic generation system," *IEEE Trans. Ind. Electron.*, vol. 55, no. 1, pp. 240–250, Jan. 2008.

[10] S. B. Kjaer, J. K. Pedersen, and F. Blaabjerg, "A review of single-phase grid-connected inverters for photovoltaic modules," *IEEE Trans. Ind. Appl.*, vol. 41, no. 5, pp. 1292–1306, Sep./Oct. 2005.

[11] "Trends in photovoltaic applications. Survey report of selected IEA countries between 1992 and 2006," Int. Energy Agency, Paris, France, Rep. IEA-PVPS T1-16, 2007.

[12] D. Sera, R. Teodorescu, and P. Rodriguez, "PV panel model based on datasheet values," in *Proc. IEEE Int. Symp. Ind. Electron.*, 2007, pp. 2392–2396.

[13] T. Esram and P. L. Chapman, "Comparison of photovoltaic array maximum power point tracking techniques," *IEEE Trans. Energy Convers.*, vol. 22, no. 2, pp. 439–449, Jun. 2007.

[14] K. Irisawa, T. Saito, I. Takano, and Y. Sawada, "Maximum power point tracking control of photovoltaic generation system under non-uniform insolation by means of monitoring cells," in *Proc. IEEE Photovoltaic Spec. Conf.*, 2000, pp. 1707–1710.

[15] K. Kobayashi, I. Takano, and Y. Sawada, "A study on a two stage maximum power point tracking control of a photovoltaic system under partially shaded insolation conditions," in *Proc. IEEE Power Eng. Soc. Gen. Meet.*, 2003, pp. 2612–2617.

[16] T. Shimizu, O. Hashimoto, and G. Kimura, "A novel high-performance utility-interactive photovoltaic inverter system," *IEEE Trans. Power Electron.*, vol. 18, no. 2, pp. 704–711, Mar. 2003.

[17] M. Calais and V. G. Agelidis, "Multilevel converters for single-phase grid connected photovoltaic systems—An overview," in *Proc. IEEE Int. Symp. Ind. Electron.*, 1998, pp. 224–229.

[18] F.-S. Kang, S.-J. Park, S. E. Cho, C.-U. Kim, and T. Ise, "Multilevel PWM inverters suitable for the use of stand-alone photovoltaic power systems," *IEEE Trans. Energy Convers.*, vol. 20, no. 4, pp. 906–915, Dec. 2005.
[19] O. Alonso, P. Sanchis, E. Gubia, and L. Marroyo, "Cascaded H-bridge multilevel converter for grid connected photovoltaic generators with independent maximum power point tracking of each solar array," in *Proc. IEEE Power Electron. Spec. Conf.*, 2003, vol. 2, pp. 731–735.
[20] J. J. Negroni, F. Guinjoan, C. Meza, D. Biel, and P. Sanchis, "Energy-sampled data modeling of a cascade H-bridge multilevel converter for grid-connected PV systems," in *Proc. IEEE Int. Power Electron. Congr.*, 2006, pp. 1–6.
[21] H. Ertl, J. Kolar, and F. Zach, "A novel multicell DC–AC converter for applications in renewable energy systems," *IEEE Trans. Ind. Electron.*, vol. 49, no. 5, pp. 1048–1057, Oct. 2002.
[22] S. Alepuz, S. Busquets-Monge, J. Bordonau, J. Gago, D. Gonzalez, and J. Balcells, "Interfacing renewable energy sources to the utility grid using a three-level inverter," *IEEE Trans. Ind. Electron.*, vol. 53, no. 5, pp. 1504–1511, Oct. 2006.
[23] J. Rodríguez, J. Lai, and F. Peng, "Multilevel inverters: A survey of topologies, controls, and applications," *IEEE Trans. Ind. Electron.*, vol. 49, no. 4, pp. 724–738, Aug. 2002.
[24] J. Rodriguez, S. Bernet, B. Wu, J. O. Pontt, and S. Kouro, "Multilevel voltage-source-converter topologies for industrial medium-voltage drives," *IEEE Trans. Ind. Electron.*, vol. 54, no. 6, pp. 2930–2945, Dec. 2007.
[25] S. Busquets-Monge, S. Alepuz, J. Bordonau, and J. Peracaula, "Voltage balancing control of diode-clamped multilevel converters with passive front-ends," in *Proc. IEEE Int. Symp. Ind. Electron.*, 2007, pp. 544–549.
[26] "Evaluation of islanding detection methods for photovoltaic utility-interactive power systems," Int. Energy Agency, Paris, France, Rep. IEA-PVPS T5-09, 2002.
[27] S. Busquets-Monge, J. Bordonau, D. Boroyevich, and S. Somavilla, "The nearest three virtual space vector PWM—A modulation for the comprehensive neutral-point balancing in the three-level NPC inverter," *IEEE Power Electron. Lett.*, vol. 2, no. 1, pp. 11–15, Mar. 2004.
[28] S. Busquets-Monge, J. Bordonau, and J. Rocabert, "Extension of the nearest-three virtual-space-vector PWM to the four-level diode-clamped dc–ac converter," in *Proc. IEEE Power Electron. Spec. Conf.*, 2007, pp. 1892–1898.
[29] I.-S. Kim, M.-B. Kim, and M.-J. Youn, "New maximum power point tracker using sliding-mode observer for estimation of solar array current in the grid-connected photovoltaic system," *IEEE Trans. Ind. Electron.*, vol. 53, no. 4, pp. 1027–1035, Jun. 2006.

Sergio Busquets-Monge (S'99–M'06) was born in Barcelona, Spain. He received the M.S. degree in electrical engineering from the Technical University of Catalonia (UPC), Barcelona, in 1999, the M.S. degree in electrical engineering from Virginia Polytechnic Institute and State University, Blacksburg, in 2001, and the Ph.D. degree in electrical engineering from UPC in 2006.

From 2001 to 2002, he was with Crown Audio, Inc. He is currently an Associate Professor with the Department of Electronic Engineering, UPC. His research interests include multilevel conversion, power-converter modeling, control and automated design, power-factor correction, and electromagnetic-interference suppression techniques.

Joan Rocabert was born in Barcelona, Spain. He received the M.S. degree in electrical engineering from the Technical University of Catalonia (UPC), Barcelona, in 2003, where he is currently working toward the Ph.D. degree in electrical engineering.

Since 2004, he has been a Researcher with the Department of Electronic Engineering, UPC. His fields of interest are in power electronics applied to photovoltaic and wind-energy systems.

Pedro Rodríguez (S'99–M'04) received the B.S. degree in electrical engineering from the University of Granada, Granada, Spain, in 1989, and the M.S. and Ph.D. degrees in electrical engineering from the Technical University of Catalonia (UPC), Barcelona, Spain, in 1994 and 2004, respectively.

In 1990, he was with the Faculty of UPC as an Assistant Professor and became an Associate Professor in 1993. He was a Researcher with the Center for Power Electronics Systems, Virginia Polytechnic Institute and State University, Blacksburg, and in the Institute of Energy Technology, Aalborg University, Aalborg, Denmark, in 2005 and 2006, respectively. He is currently the Head of the Research Group on Renewable Electrical Energy Systems, Department of Electrical Engineering, UPC. He has coauthored about 100 papers in technical journals and conferences. He holds two patents. His research interests include power conditioning, integration of distributed energy systems, and control of power converters.

Dr. Rodríguez is a member of the IEEE Power Electronics, IEEE Industrial Electronics, and IEEE Industry Applications Societies.

Salvador Alepuz (M'03) was born in Barcelona, Spain, in 1967. He received the M.Sc. and Ph.D. degrees in electrical and electronic engineering from the Technical University of Catalonia (UPC), Barcelona, Spain, in 1993 and 2004, respectively.

Since 1994, he has been an Associate Professor with the Department of Electronic Engineering, UPC. From 2006 to 2007, he was with the Departamento de Electrónica, Universidad Técnica Federico Santa María, Valparaíso, Chile, where he was developing a postdoctoral research. His fields of interest are in multilevel conversion and ac-power conversion applied to renewable-energy systems.

Josep Bordonau (S'87–M'89) received the M.Sc. and Ph.D. degrees (with honors) in electrical engineering from the Technical University of Catalonia (UPC), Barcelona, Spain, in 1984 and 1990, respectively.

He was a Lecturer and an Assistant Professor with the Electronics Engineering Department, UPC, where he has been an Associate Professor since 1991. He has been active in more than 25 research projects with international companies and institutions. He has authored more than 60 journal and conference papers. His fields of interest are in multilevel conversion and ac-power conversion applied to renewable-energy systems and energy-management systems.